Available online at www.sciencedirect.com
ScienceDirect
International Journal of Thermal Sciences 47 (2008) 918–925
International Journal of Thermal Sciences
www.elsevier.com/locate/ijts

Experimental study of natural convection in a glass pool inside a cold crucible induction melter

G. Sugilal *

Nuclear Recycle Group, Bhabha Atomic Research Centre, Trombay, Mumbai-400085, India

Received 29 April 2007; received in revised form 20 June 2007; accepted 20 June 2007

Available online 2 August 2007

Abstract

Cold crucible induction melting is evolving as a promising technology for vitrification of high level radioactive waste because of high temperature availability and long melter life. Natural convection in the inductively heated glass pool plays a significant role in the performance of such melters. Experimental investigations were carried out to study the nature of flow patterns and temperature profiles in a sodium borosilicate glass pool inside an engineering scale cold crucible induction melter. Flow patterns were obtained for power levels in the range of 50 to 110 kW. The average surface velocity was found to vary from 5 mm s^{-1} at 50 kW to 22.5 mm s^{-1} at 110 kW. Experimentally measured temperature profiles in the glass pool indicated a well-mixed zone above a thermally stratified layer.

Keywords: Cold crucible induction melter; Glass melting; Natural convection; Vitrification

1. Introduction

In 1926, a German Patent (No. 518,499) proposed the use of water-cooled, segmented metal crucible to melt refractory metals by an induction coil surrounding the crucible. A similar melter was developed later by Schippereit (US Patent No. 3,223,519) employing a non-conductive slag material between the molten metal and the segmented metallic vessel. Although this melter was successful on a smaller scale, larger systems ended in failures due to molten metal shorting across the segmented crucible. However, induction melting in cold crucible was widely utilized in Russia in the 1970s for the production of oxide-based refractories [1]. In 1980s, inducto-slag melting process was scaled up successfully for use in producing titanium castings employing larger, multi-segmented crucible with a 350 kW, 3 kHz induction power supply [2]. The Cold Crucible Induction Melting (CCIM) process, also known as Induction Skull Melting (ISM) process, is widely used to produce high purity melts of a range of difficult to melt materials, including Ti–Al alloys for aerospace applications, high temperature superconducting materials and silicon for electronic applications, corium (a mixture of UO_2 and ZrO_2) for nuclear reactor applications etc. Experimental investigations of cold crucible induction melting of metals were carried out by many researchers in order to study various aspects of design and operation of such systems [3–5]. Similar studies for melting non-metallic, refractory materials were also reported in the open literature [6–8].

Cold crucible induction melting is globally emerging as an alternative technology for the vitrification of high level radioactive waste as it offers several advantages such as high temperature availability with long melter life, high waste loading, high specific capacity etc. Research and development studies related to application of CCIM technology for immobilization of high level radioactive wastes are in progress in countries like France [9], Russia [10] and USA [11].

In cold crucible induction glass melting, glass is directly heated by electromagnetic induction employing a segmented crucible which is manufactured from contiguous segments forming a cylindrical volume, but separated by a thin layer of electrically insulating material [12]. An inductor surrounding the segmented crucible induces eddy currents in each segment creating an electromagnetic field inside the crucible. Such an arrangement is equivalent to two air-cored transformers—one

* Tel.: +91 22 25591074; fax: +91 22 25505151.
E-mail address: gsugilal@gmail.com.

1290-0729/$ – see front matter
doi:10.1016/j.ijthermalsci.2007.06.017

Nomenclature

I	Feeder line current to induction heating power supply ..... A	T	glass temperature ..... °C
P	input power to the melter ..... W	T_1	temperature at $R = 180$ mm, $Z = 270$ mm ... °C
R	radial location of a thermocouple ..... mm	T_2	temperature at $R = 0$ mm, $Z = 270$ mm ..... °C
t	melter operating time ..... s	V	glass velocity ..... $m\,s^{-1}$
		Z	axial (vertical) location ..... mm

formed by the induction coil and the crucible segments and the second formed between the segments and the charge. Thus, the segmented crucible acts as a field concentrator, indirectly reducing the gap between the induction coil and the charge. Direct heating of glass facilitates heating the process material to high temperatures. In order to avoid high temperature glass corrosion of the metallic crucible, internal cooling of the segments is provided. This cooling produces a solidified glass layer, which acts as a protection against glass corrosion along the melter inner wall. High temperature availability without substantial corrosion makes the CCIM a promising technology for immobilization of high level nuclear waste. Based on the laboratory and bench scale experimental studies carried out at Bhabha Atomic Research Centre, an engineering scale cold crucible induction melter (ESCCIM) was indigenously developed for technology demonstration [13]. In the present paper, results of an experimental study of natural convection in molten glass pool inside the ECCIM are described. The overall objective of the present investigations was to study the convective behaviour of the molten glass pool under different operating power levels. The melter performance is strongly linked to the thermal and flow field in the glass melt. Therefore, a better understanding of the natural convection in the glass melt is essential for the design and operation of the CCIM for such applications.

2. Engineering scale experimental facility

The experimental facility, shown in Fig. 1, comprises of an engineering scale cold crucible induction melter, an induction heating system and a heat removal system. Major components of the ESCCIM are shown in Fig. 2. The melter essentially has a water-cooled base to support the molten mass, a circular array of electrically isolated segments to facilitate electromagnetic field penetration into the melter and an inlet–outlet chamber to provide cooling water to the vertical segments, which constitute the melter wall. The ESCCIM comprises of 56 segments with a tube-in-tube configuration. Each of these segments consists of a one inch outer tube (BWG 12) connected to the cooling water inlet chamber and a half inch inner tube (BWG 12) connected to the cooling water outlet chamber. These stainless steel cooling tubes are arranged in a circular array to hold a molten glass pool of 500 mm diameter. The base and the tubular segments are electrically isolated with a 3 mm thick Teflon gasket in order to avoid electrical short-circuiting of the segments at the bottom. An inlet ring header is employed to distribute cooling water to the lower inlet chamber and an outlet ring header connected to upper outlet chamber is used to discharge hot water from the

Fig. 1. Engineering Scale Cold Crucible Induction Melter (ESCCIM).

melter. The base is provided with an independent cooling water circuit. A water-cooled mechanical plug assembly protruding 200 mm above from the melter floor is used to drain molten glass from the melter. All metallic parts of the crucible were fabricated out of nitric acid grade stainless steel (SS 304L) considering the acidic nature (3 M HNO_3) of the high level liquid waste.

An indigenously available, transistor-based induction heating power supply system with an operating frequency of 200 kHz was chosen for the present ESCCIM application. This power supply, procured from M/s. G. H. Induction India Pvt. Ltd., provides diameter to skin-depth ratios ranging from 2 to 4.5 for different glasses with electrical conductivities ranging from 5 to 1 Ohm cm. A current-fed, parallel resonant load circuit was selected for the inverter circuit topology. The inverter was rated for 350 kW with a maximum power delivery of 200 kW in the load. A one-turn, 3 mm thick, 220 mm high,

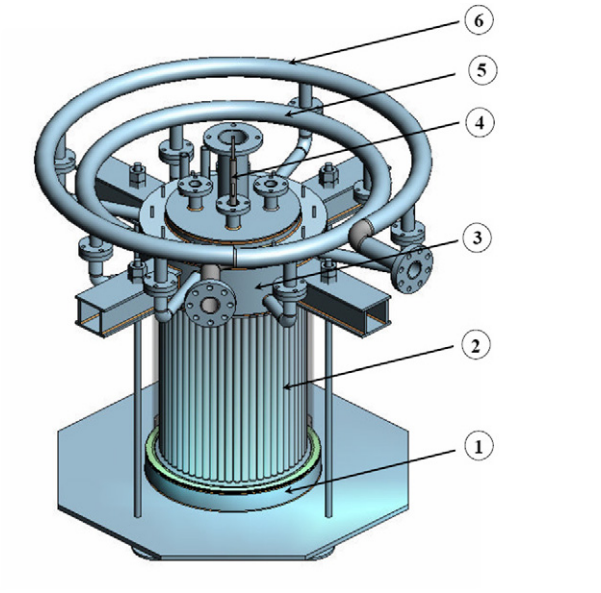

1 water-cooled base
2 water-cooled segments
3 cooling water inlet-outlet chamber
4 water-cooled mechanical plug
5 cooling water inlet header
6 cooling water outlet header

Fig. 2. Major components of the ESCCIM.

water-cooled copper inductor was used to limit the maximum coil voltage requirement to 1600 V. A coil inside diameter of 600 mm was chosen to provide a 25 mm thick casting of high temperature refractory cement on the exterior of the crucible segments. The coil was located 150 mm above from the water cooled base of the ESCCIM to reduce the Joule heat generation in the top metallic plate of the base. A 5 m long water-cooled, copper busbar was used to connect the inductor and the capacitor bank.

The heat removal system comprises of primary cooling water (PCW) circuit which cools various components of the segmented ESCCIM and secondary cooling water (SCW) circuit which removes the heat gained by the PCW from the melter. The PCW loop consists of a plate type heat exchanger (heat duty: 200 kW) and a stainless steel centrifugal pump (capacity: 750 LPM, head: 35 m) and a DM water storage tank. The SCW circuit consists of a cooling tower (heat duty: 250 kW) and a circulation pump (capacity: 1000 LPM, head: 35 m) in addition to the heat exchanger connected to the PCW loop. Adequate instrumentations such as flow rate and temperature measurements were provided to generate sufficient engineering data for design verification.

3. Experimental procedure

Sodium borosilicate glass with chemical composition given in Table 1 was used for the present study. Electrical conductivity and viscosity of this glass are given in Tables 2 and 3 respectively. Glass being an electrical insulator at room temperature, it must be preheated enough for substantial electromagnetic coupling and sustained induction heating. Graphite rings (of 50 mm outside diameter, 30 mm inside diameter and 10 mm height) were used for start-up heating. A chain formed from 25 to 40

Fig. 3. Melter inside view during melter start-up.

Table 1
Composition of sodium borosilicate glass

Chemical	Weight %
SiO_2	32
B_2O_3	25
Na_2O	28
Fe_2O_3	13
TiO_2	2

Table 2
Electrical resistivity of sodium borosilicate glass

Temperature (°C)	Resistivity (Ohm cm)
900	3.3
1000	1.9
1100	1.2

Table 3
Viscosity of sodium borosilicate glass

Temperature (°C)	Viscosity (Poise)
850	72.5
900	39.4
950	13.2
1000	9.4
1050	8.2

graphite rings was placed at the top centre of the initial charge of 90 kg of glass frit of 5–10 mm size. The rectifier output voltage was set to 350 V (dc) to produce 80 kW in the load. Melter inside view during the start-up is shown in Fig. 3. The glass melt grows gradually from the centre to the periphery. The line current to the induction heating power supply increases substantially as the electromagnetic coupling with the molten glass improves and finally reaches a steady state for a given power level. In order to establish the required glass level, prefabricated glass frits of 5–10 mm size was fed onto the surface of the molten glass pool using a vibratory feeder.

An array of three inconel-sheathed, N-type thermocouples in ceramic thermowells (6 mm inside diameter and 3 mm thick),

1 Mechanical plug
2 Thermowell at R = 0 mm
3 Thermowell at R = 90 mm
4 Thermowell at R = 180 mm

Fig. 4. Arrangement of ceramic thermowells inside the ESCCIM.

as shown in Fig. 4, was used to obtain the radial and vertical temperature profiles in the molten glass pool. The thermocouple array was lifted up gradually to measure the glass temperatures at a vertical interval of 10 mm. The convective flow patterns at different power levels were obtained using a digital camera. The velocity of glass flow on the pool surface was experimentally determined by noting the average time taken by floating glass beads of 3 mm diameter to travel from the melter periphery to the top centre.

4. Experimental results

Two independent runs were conducted to study the impact of operational history and operating power level on the thermal field in the glass melt. Operational history of run 1 is shown in Fig. 5. The melter was initially filled up to a level of 200 mm with 90 kg of glass frit. A chain formed from 25 graphite rings was used for the melter start-up heating which took about 4 hours to produce sufficient pool for substantial electromagnetic coupling. Additional 40 kg of glass was added to obtain a final molten glass level of 290 mm. Operating power level was maintained at 90 kW and the pool was allowed to reach steady-state. The melt depth at the pool periphery was measured to be 165 mm using a dip-stick method. The average glass surface temperature at 90 kW was 1050 °C. Fig. 6 shows the steady-state temperature profiles in the molten glass pool corresponding to run 1. These temperature profiles indicate a stable thermal stratification below 200 mm glass level where relatively quiescent glass pool is expected. Model predictions of Hawkes [14] also show the existence of thermally stratified layer in the glass pool inside a cold crucible induction heated melter for melting radioactive waste glass. Two different body forces (viz., electromagnetic body force due to the high frequency coil current and gravitational body force due to the non-uniform thermal field) prevail in an induction-heated, electrically conducting liquid. The convective behaviour of the liquid pool under induction heating depends strongly on the relative magnitudes of the two body forces. In general, electromagnetically driven flows occur in metal melting applications

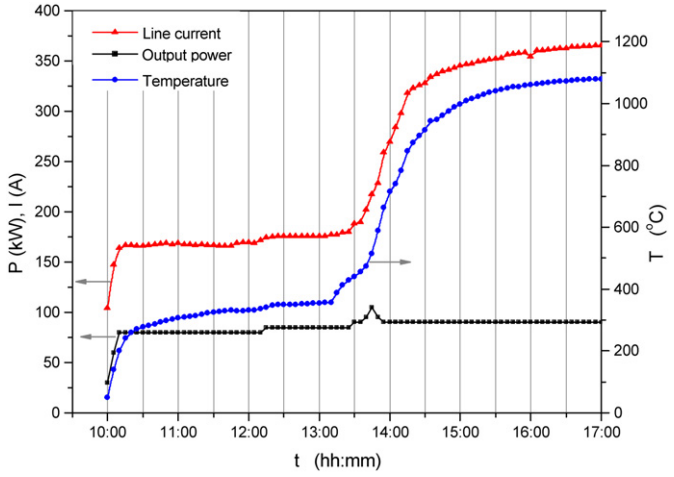

Fig. 5. Operational history of run 1.

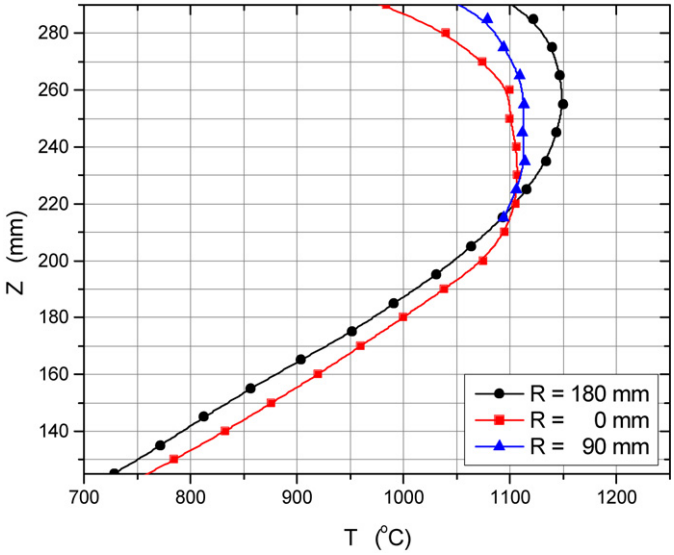

Fig. 6. Temperature profiles in the glass pool (run 1).

in which the flow is predominantly in the radially outward direction at the pool surface and gravity-driven flows occur in glass melting applications in which the flow is predominantly in the radially inward direction at the surface. In the present study, thermal stratification was observed in the lower part of the glass pool where temperature varies almost linearly with height. In this stably stratified thermal layer of the glass melt, wherein temperature increases with height, the heat transfer is essentially by means of thermal conduction. Experimental results of internal gravity-driven flows in a volumetrically heated melt accumulation bounded by cold walls indicate similar thermal stratification [15]. In the present design, a water-cooled mechanical plug protrudes 200 mm above from the melter base so that the well-stirred glass above it can be drained to ensure product homogeneity. The quiescent glass pool is always maintained as heat source for the next batch subsequent to every glass pouring. In the thermally stratified zone of run 1, the temperature at the centre was observed to be higher than that near the periphery on account of the prolonged heating at the centre

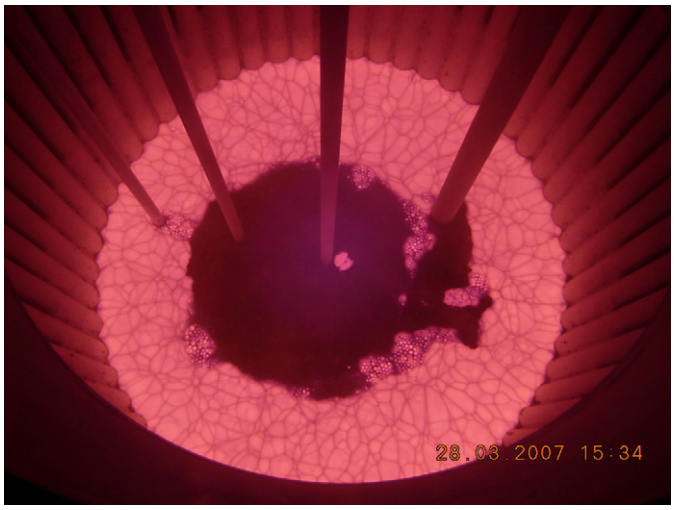

Fig. 7. Pool surface conditions and flow pattern during glass melting.

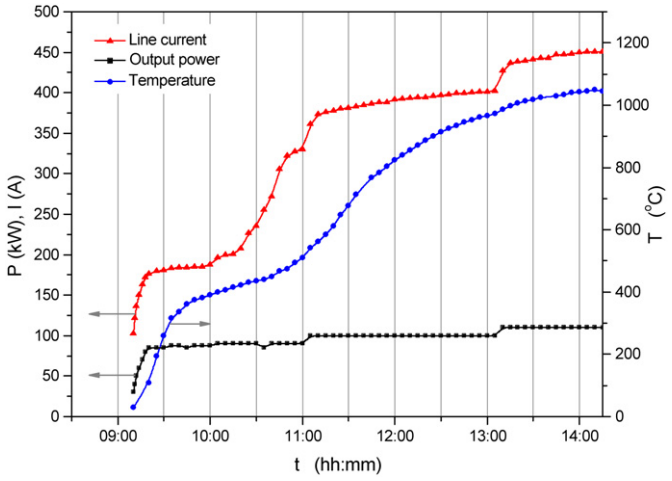

Fig. 8. Operational history of run 2.

during melter start-up. In the upper part of the pool, glass at the periphery is hotter due to the skin effect.

During the experiment, glass melting rate was observed to vary strongly with the melter operating power as expected. The melting rates varied from 20 kg h^{-1} at a power level of 90 kW to 40 kg h^{-1} at 110 kW. The melting rate was enhanced by better mixing on account of the stronger natural convection currents in the molten glass pool. The surface conditions and the convective flow patterns during glass melting are shown in Fig. 7.

In order to study the impact of melter operating power on the flow pattern and temperature profiles in the glass pool, an independent experiment was carried out. The operational history of run 2 is given in Fig. 8. Initial conditions of the second run were identical to those of the first run except that a chain of 40 graphite rings was used to accomplish a faster melting. Total glass used in run 2 was 140 kg instead of 130 kg in run 1. The final molten glass level in run 2 was measured to be 300 mm with a glass pool depth of 175 mm at the pool periphery. The operating power level was set to 110 kW and the glass pool was allowed to reach steady state. The temperature profiles for 110 kW are shown in Fig. 9. (Thermocouple at $R = 90$ mm

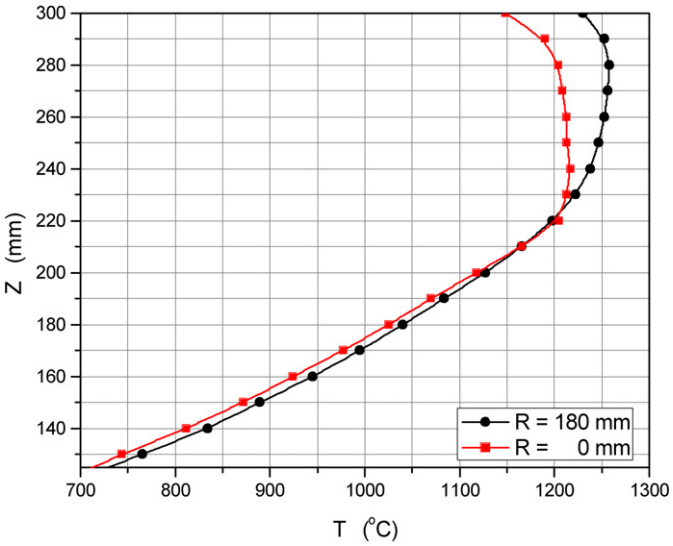

Fig. 9. Temperature profiles in the glass pool (run 2).

was not functional during run 2.) The average surface temperature at this power level was 1200 °C. Fig. 9 shows that the thermal field at the centre of the pool is more uniform than that at the periphery, suggesting a stronger flow at the centre. Numerical simulation results obtained by Hawkes [14] confirm the presence of a stronger flow field at the centre of the glass pool. Fig. 9 also indicates stable thermal stratification similar to that of run 1. However, thermal field in the pool above the quiescent layer appears to be more uniform on account of the stronger convection currents at higher operating power. In metal melting applications, it is difficult to maintain melt superheat even though the power is increased [5]. This is due to the fact that the enhanced electromagnetically driven flow, due to the increase in power, results in additional heat loss to the cold crucible. High convection currents (with velocities of the order 10^{-1} m s^{-1}) in the melt and high thermal conductivity (of the order of 10^{2} W m^{-1} K^{-1}) of the metallic skull make superheating of the molten metal difficult. In glass melting application, the heat loss in the thermally stratified lower zone is governed by conduction and that in the upper zone is governed by the thermally induced natural convection. High viscosity of molten glass (with velocities of the order 10^{-2} m s^{-1}) and low thermal conductivity (of the order of 1 W m^{-1} K^{-1}) of the solidified glass layer lead to relatively lower crucible losses when compared to that in a molten metal. These aspects explain the observed rise in the molten glass pool temperature with increase in power.

The thermal conditions and flow patterns at the glass pool surface were recorded for different power levels using a digital camera. These photographs are presented in Fig. 10, which clearly indicates that the thickness of the solidified glass layer near the pool periphery decrease with increasing power levels signifying an increase in the heat loss from the pool to the water-cooled segments of the crucible. Skin effect caused by the high frequency magnetic field results in a relatively hotter glass at the periphery of the molten glass pool. As a result, lighter glass rises at the periphery and flows towards the cen-

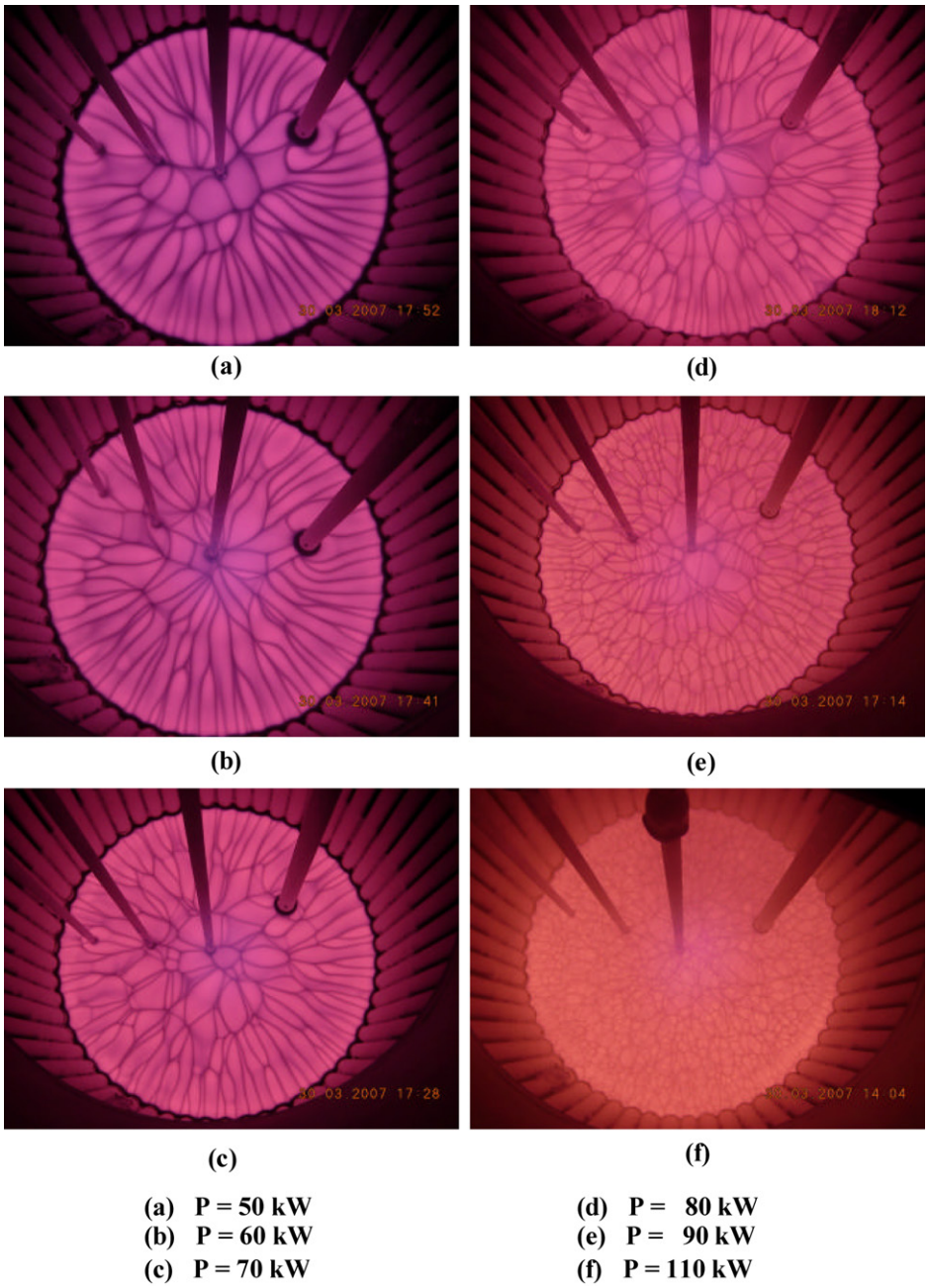

Fig. 10. Flow patterns at different melter power (run 2).

tre of pool surface. As it flows along the pool surface, it looses heat to the surrounding leaving the glass cooler near the centre where the denser glass sinks. Enhanced operating power improves net gravitational body forces; weakens the resistive viscous forces; and thereby results in better mixing. It is expected that the electromagnetic body forces prevailing in the poorly conducting glass pool is not strong enough to contribute to the natural convection significantly.

Flow patterns presented in Fig. 10 show that moderately ordered radial flow from the pool periphery to the centre prevails at low power level. (The ceramic thermowells and water-cooled mechanical plug certainly interfere with the flow patterns.) The streaks which appear on the glass surface are formed by relatively cold glass drawn from the melter periphery by the convection currents. These streaks are comparatively longer at low power level and the neighbouring streaks join together towards the centre of the pool. As the power level increases, the number of streaks increases with more and more and more cross connections get established. The flow becomes more chaotic at higher power levels. The velocity of glass flow on the pool surface was experimentally determined by noting the average time taken by floating glass beads of 3 mm diameter to travel from the melter periphery to the top centre. The velocities thus obtained for different power levels are plotted in Fig. 11. The velocity grows exponentially with increase in power. The average surface velocity was found to vary from 5 mm s^{-1} at 50 kW

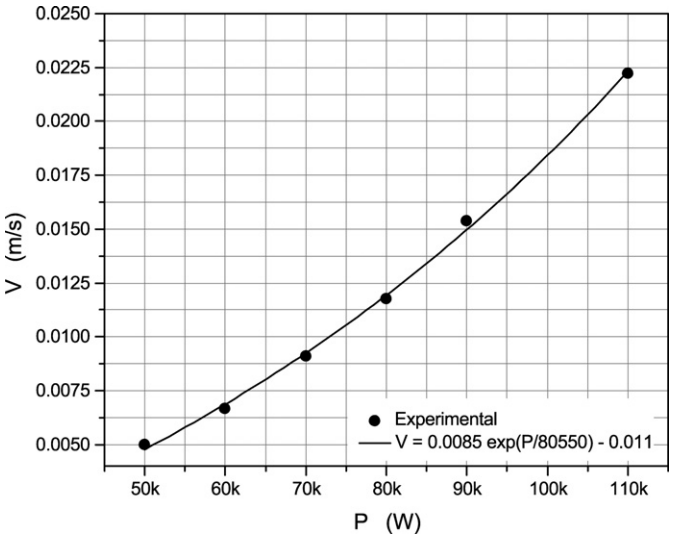

Fig. 11. Glass velocity at different melter power (run 2).

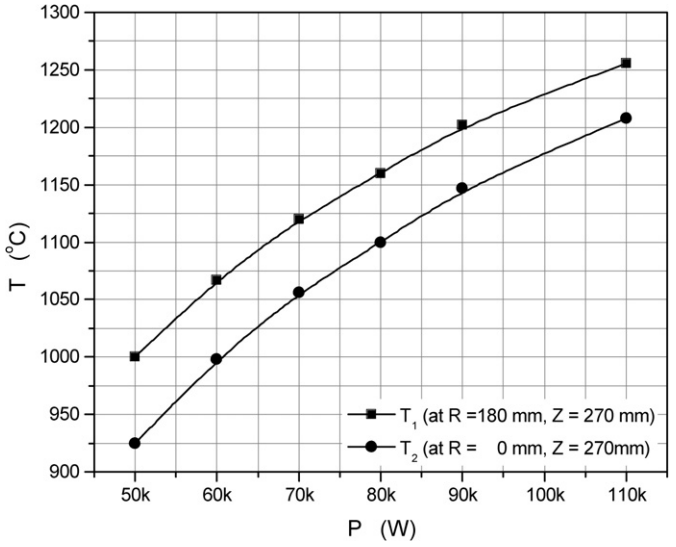

Fig. 12. Glass temperature at different melter power (run 2).

to 22.5 mm s^{-1} at 110 kW. The exponential relation shown in Fig. 11 concurs with the experimental results with in a maximum error of 3.75%.

In Fig. 12, glass temperatures at two different radial locations ($R = 0$ and $R = 180$ mm) on the same horizontal plane (270 mm from the bottom) are plotted to show the impact of operating power on the thermal field prevailing in the glass pool. Fig. 12 shows that the difference between the two temperatures decreases, as expected, with increase in power. As the differential temperature across two fixed points in the glass pool decrease with improved mixing on account of buoyancy induced natural convection, the ratio of power to the differential temperature can be used to represent the degree of mixing in the glass pool. Such an index can be used to indicate the product homogeneity. Since the glass velocity is governed by the strength of the convection currents in the pool, a linear relation can be expected between the measured velocity and the ratio of the power to differential temperature. Fig. 13, in which measured velocity is plotted against $[P/(T_1 - T_2)]$ ratio for power levels ranging from 50 to 110 kW, proves this guess. The linear relationship shown in Fig. 13 fits the experimental results with in a maximum error of 3.36%.

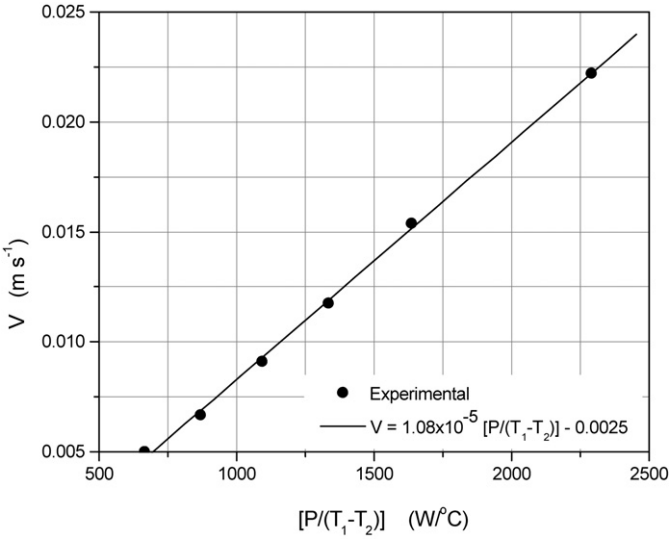

Fig. 13. Glass velocity versus ratio of power to differential temperature (run 2).

Convective behaviour of the molten glass pool inside the CCIM can be analysed in detail using a mathematical model involving Maxwell's equations describing the electromagnetic field and the Navier–Stokes equations describing the flow and thermal fields. Such a study will be carried out to investigate the effect of different parameters such as variable properties, surface tension, electromagnetic body forces (also known as Lorentz force) etc. on the performance of CCIM used for glass melting applications.

5. Conclusions

Convective behaviour of an electrically conducting molten glass pool inside an engineering scale cold crucible induction melting was investigated experimentally using sodium borosilicate glass. Flow patterns obtained for different power indicate that turbulent conditions prevail under the normal operating conditions of the melter. Temperature profiles in the molten glass pool show that a well-mixed zone exists above a thermally stratified layer of molten glass. The average surface velocity was found to vary from 5 mm s^{-1} at 50 kW to 22.5 mm s^{-1} at 110 kW. The melting rate was enhanced by better mixing on account of the stronger natural convection currents in the molten glass pool. The melting rates varied from 20 kg h^{-1} at a power level of 90 kW to 40 kg h^{-1} at 110 kW.

Acknowledgements

Technical contributions by J.G. Shah in providing the compositions and physical properties of glass are gratefully acknowledged. The author is also grateful to S.D. Misra, Director, Nuclear Recycle Group for his constant support and to C. Srinivas for the useful discussions.

References

[1] Yu.B. Petrov, A.E. Slukhotskii, A.V. Shkul'kov, Investigation of cold crucible induction melting in production of refractory electrical-grade materials for electrothermics, Electroteckhnika 52 (1981) 55–59.

[2] D.J. Chronister, S.W. Scott, D.R. Stickle, Induction melting of titanium, zirconium, and reactive alloys, in: Proceedings of the 1986 Vacuum Metallurgy Conference on Specialty Metals Melting and Processing, Pittsburgh, Pennsylvania, USA, 1986, pp. 7–10.

[3] F. Negrini, M. Fabbri, M. Zuccarini, E. Takeuchi, M. Tani, Electromagnetic control of meniscus shape during casting in a high frequency magnetic field, Energy Conversion & Management 41 (2000) 1687–1701.

[4] M. Vogt, F. Bernier, A. Muhlbauer, M. Blum, G. Jarczyk, Experimental investigations of temperature field and energy flows in induction furnace with cold crucible and a practical application of the results, in: Proceedings of International Symposium on Electromagnetic Processing of Materials, Nagoya, Japan, 2000, pp. 289–294.

[5] V. Bojarevics, R.A. Harding, K. Pericleous, M. Wickins, The development and experimental validation of a numerical model of an induction skull melting furnace, Metallurgical and Materials Transactions B 35 (2004) 785–830.

[6] T. Behrens, M. Kudryash, B. Nacke, D. Lopukh, A. Martynov, I. Loginov, Induction skull melting of Y_2O_3–BaO–CuO in a cold crucible, in: Proceedings of International Scientific Colloquium on Modelling of Electromagnetic Processing, Hannover, Germany, 2003, pp. 249–254.

[7] J.H. Sing, B.T. Min, J.H. Kim, H.W. Kim, S.W. Hong, S.H. Chung, An electromagnetic and thermal analysis of a cold crucible melting, International Communications in Heat and Mass Transfer 32 (2005) 1325–1336.

[8] S.W. Hong, B.T. Min, J.H. Song, H.D. Kim, Application of cold crucible for melting of UO_2/ZrO_2 mixture, Materials Science and Engineering A 357 (2003) 297–303.

[9] R. Do Quang, A. Jensen, A. Prod'homme, R. Fatoux, J. Lacombe, Integrated pilot plant for a large cold crucible induction melter, in: Proceedings of the Waste Management 2002 Symposium, Tucson, USA, 2002.

[10] F.A. Lifanov, M.I. Ojovan, S.V. Stefanovsky, R. Burcl, Feasibility and expedience to vitrify NPP operational waste, in: Proceedings of the Waste Management 2003 Symposium, Tucson, USA, 2003.

[11] D. Gombert, J.R. Richardson, J.A. Roach, N.R. Soelberg, Cold crucible induction melter prototype at the Idaho National Engineering and Environmental Laboratory, in: Proceedings of the Waste Management 2004 Symposium, Tucson, USA, 2004.

[12] A. Jouan, R. Boen, S. Merlin, P. Roux, A warm heart in a cold body—melter technology for tomorrow, in: Proceedings of the Spectrum 96, International Topical Meeting on Nuclear and Hazardous Waste Management, Seattle, USA.

[13] G. Sugilal, P.K. Wattal, Development of cold crucible induction melting technology for vitrification of high level liquid waste, in: Proceedings of 14th Annual Conference of INS and 1st BRNS Conference on Nuclear Fuel Cycle, Kalpakkam, India, 2003.

[14] G. Hawkes, Modelling a cold crucible induction melter, in: Proceedings of 2003 FIDAP/POLYFLOW Users Group Meeting, Evanston, Illinois, USA, 2003.

[15] S.D. Lee, K.Y. Suh, Natural convection heat transfer in two-dimensional semicircular slice pool, Journal of Nuclear Science and Technology 40 (2003) 775–782.